Design, characterization and model validation of a LED-based photocatalytic reactor for gas phase applications

Khodadadian, Fatemeh; de Boer, Merijn W.; Poursaeidesfahani, Ali; van Ommen, J. Ruud; Stankiewicz, Andrzej I.; Lakerveld, Richard

DOI
10.1016/j.cej.2017.09.108

Publication date
2018

Document Version
Final published version

Published in
Chemical Engineering Journal

Citation (APA)
Khodadadian, F., de Boer, M. W., Poursaeidesfahani, A., van Ommen, J. R., Stankiewicz, A. I., & Lakerveld, R. (2018). Design, characterization and model validation of a LED-based photocatalytic reactor for gas phase applications. *Chemical Engineering Journal*, *333*, 456-466. https://doi.org/10.1016/j.cej.2017.09.108

Chemical Engineering Journal 333 (2018) 456–466

Contents lists available at ScienceDirect

Chemical Engineering Journal

journal homepage: www.elsevier.com/locate/cej

Design, characterization and model validation of a LED-based photocatalytic reactor for gas phase applications

Fatemeh Khodadadian[a], Merijn W. de Boer[b], Ali Poursaeidesfahani[a], J. Ruud van Ommen[b], Andrzej I. Stankiewicz[a], Richard Lakerveld[c,*]

[a] Department of Process & Energy, Delft University of Technology, Leeghwaterstraat 39, 2628 CB Delft, The Netherlands
[b] Chemical Engineering Department, Delft University of Technology, Van der Maasweg 9, 2629 HZ Delft, The Netherlands
[c] Department of Chemical and Biomolecular Engineering, The Hong Kong University of Science & Technology, Clear Water Bay, Kowloon, Hong Kong

GRAPHICAL ABSTRACT

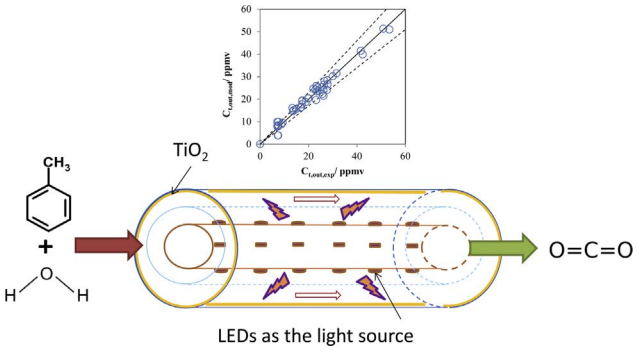

ARTICLE INFO

Keywords:
Photocatalysis
Light emitting diodes
Volatile organic compounds
Parameter estimation
Model validation
Toluene oxidation

ABSTRACT

The design and operation of reactors for photocatalytic degradation of organic pollutants remains challenging due to the complex interplay of photon, mass, and heat transfer. An integrated process model including a radiation field, reaction kinetics, and material balances of an annular LED-based photocatalytic reactor for photocatalytic degradation of toluene is validated using experimental data from a mini-pilot plant. A particular emphasis is on the effect of water on reaction kinetics, toluene conversion, mineralization, and catalyst deactivation, which is currently not well understood. The results from parameter estimation demonstrate that a competitive reaction rate model describes the experimental data with varying water concentration best. Furthermore, experimental trends demonstrate that toluene conversion is highest at low water concentrations, however, mineralization and catalyst lifetime are enhanced by the presence of water. The validation of the integrated process model and understanding of the role of water allow for improved design and operation of future photocatalytic reactors.

1. Introduction

Heterogeneous photocatalysis has great potential for many applications involving either a liquid or a gas phase [1–5]. Photocatalysis uses a semiconductor, often TiO_2, to generate catalytic active sites by absorbing photons that are typically in the UV range. Recently, much attention has been paid to the capability of this technology for remediation of water and air because of its ability to degrade a broad

* Corresponding author.
E-mail address: kelakerveld@ust.hk (R. Lakerveld).

http://dx.doi.org/10.1016/j.cej.2017.09.108
Received 26 April 2017; Received in revised form 16 September 2017; Accepted 18 September 2017
Available online 22 September 2017
1385-8947/

range of organic pollutants at very low concentrations [6–9]. However, photocatalysis still lacks broad industrial adoption due to its low overall efficiency despite its promising applications and intensive research during the last decades.

The main challenges to improve the efficiency of photocatalytic processes include the development of more efficient photocatalysts as well as the design of efficient photocatalytic reactors. The latter is complicated by the lack of knowledge on kinetic reaction mechanisms and by the need to optimize mass, heat, and photon transfer simultaneously [10,11]. Especially, if artificial light sources are used, an efficient utilization of photons within the reactor is of great importance to lower operational costs while still achieving optimal illumination of the catalyst. Furthermore, efficient mass transfer of reactants and products is required. Therefore, the scale-up and efficient operation of photocatalytic reactors remains challenging, which may hinder commercial development [10].

Mathematical models based on first principles can be efficient tools for design, scale-up and optimization studies since process models provide an understanding about optimal performance and limitations of a process. For photocatalytic processes, such models should include mass, momentum and radiation balances coupled via reaction kinetics. Several studies have been dedicated to modelling of photocatalytic systems for different applications [12–19]. Tomasic et al. [13] compared one (1-D) and two-dimensional (2-D) models of a continuous annular photocatalytic reactor for toluene degradation in air, where TiO_2 was coated on the inner wall of the reactor shell and illuminated internally by a fluorescent blacklight blue lamp. They concluded that a 2-D model is superior to a 1-D model when comparing experiments to simulations. Lopes et al. [14] modelled a continuous tubular photocatalytic reactor, under simulated solar irradiation assuming a uniform light distribution on the catalytic surface, for degradation of perchloroethylene over TiO_2 in the gas phase by solving mass and momentum balances. They combined the mathematical model with different reaction rate expressions and fitted to the experimental results from a lab-scale set-up to find the mechanism that described the reaction best. In general, the irradiance over the catalyst surface might not be uniform leading to differences in local reaction rates. Therefore, a radiation field model predicting the local photon flux within the reactor is important to improve models of photocatalytic processes [15,18]. Hossain et al. [17] developed a three-dimensional model for a pilot-plant monolith photocatalytic reactor, which was illuminated from the front and back sides by low pressure mercury lamps. The model included mass, momentum and radiation balances and was validated experimentally for degradation of formaldehyde and toluene. A monolith reactor provides a large catalytic surface area; however, the photon utilization within such a reactor can be poor. In order to provide a bigger catalytic surface area and more efficient photon utilization, Imoberdorf et al. [16] proposed a multi-annular photocatalytic reactor, where TiO_2 is coated on the reactor walls. They studied models and experiments of the reactor for perchloroethylene photocatalytic degradation in air. A tubular UV lamp was placed at the center of the reactor and the lamp emission profile was modelled and coupled to intrinsic reaction rates to close material balances and a momentum balance. The experimental data corresponded well to the model. In another study, Batista et al. [19] modelled the performance of a non-steady state annular photocatalytic reactor, illuminated externally by four cylindrical daylight fluorescent lamps. The model was validated by experimental results for toluene degradation over CeO_2-TiO_2. Experimental results confirmed the results from the model.

Conventional lamps, which are frequently applied for photocatalysis studies, are normally rigid cylindrical lamps constraining the reactor design due to their fixed shape and size. In addition, they exhibit a relatively short life span, high toxicity, risk for gas leakage and disposal issues, and a relatively high energy consumption and heat production [20]. When using artificial light sources, the operational costs of a photocatalytic process are mainly determined by photon generation. Therefore, an inefficient photon generation and utilization within a reactor may limit economic viability. Alternatively, Light emitting diodes (LEDs) are feasible light sources for TiO_2 assisted-photocatalytic applications [21,22]. Compared to conventional lamps, LEDs are more robust, energy efficient, cheap, non-toxic, long-lasting and compact. Moreover, cost might be favoured by a non-uniform illumination, which cannot be achieved easily with a conventional lamp [23]. Finally, LEDs are small, which offers flexibility for design and, therefore, require a systematic design approach when used in photocatalytic reactors.

Modelling of a LED-based photocatalytic reactor including an emission model for LEDs to derive the local rate of photon absorption is important for design and optimization, but only few studies exist on this topic. Wang et al. [24] modelled an externally illuminated flat plate photocatalytic reactor for degradation of dimethyl sulphide. A flat array of 3×9 LEDs, whose dimension matched the TiO_2 catalytic plate inside the reactor, was chosen as the light source in this study. A LED emission model was coupled with reaction kinetics and computational fluid dynamics (CFD) to model the degradation of dimethyl sulphide in air, which showed good agreement with experiments. Most of the experimental studies on modelling and validation of photocatalytic processes have been done using lab-scale photocatalytic reactors. However, considering the complicated scale dependency of photon and mass transfer within photocatalytic reactors, studies on the modelling and experimental validation of larger scale LED-based photocatalytic reactors are also needed.

The objective of this work is to validate experimentally an integrated process model of a LED-based photocatalytic reactor on a mini-pilot plant scale. An experimental setup involving an internally illuminated annular LED-based photocatalytic reactor was designed and constructed for the current model validation study using the photocatalytic degradation of toluene, a typical indoor air pollutant, in the gas phase as model system. Toluene is one of the most common indoor pollutants, which has recently raised many concerns regarding human health [4,25–27]. The process model has been described and optimized in earlier work [23] and includes mass transfer, reaction kinetics, and a LED emission model. The mass transfer model and radiation field model allow for local concentrations of chemical species and photon absorption to be calculated when kinetics of toluene degradation are fully understood. In addition to toluene and oxygen, water will likely be part of the feed mixture of any practical system. However, although the role of water in photocatalytic degradation of toluene has been investigated extensively [28–35], water remains a controversial subject of debate. Some studies showed that in the absence of water, no photocatalytic degradation of toluene occurs [30–34], while other studies proposed only a minor role of hydroxyl radicals originated from water in the photocatalytic degradation of toluene[28,29,35]. The effect of water on the process behaviour of a LED-based photocatalytic reactor needs to be fully understood to develop reliable process models for engineering purposes such as design, control, and optimization. Therefore, this study aims to improve the prediction of the effect of water by operating the system at different relative humidity and fitting various kinetics models to the data from the new mini-pilot plant. Furthermore, a focus will be on the experimental trends regarding conversion and full mineralization of toluene and catalyst deactivation as function of water content. Catalyst deactivation has been reported frequently in related studies at high toluene concentrations [30,36]. Finally, the effect of other variables such as toluene inlet concentration, residence time, and irradiance will be investigated to better understand process trends and to create a data set that is sufficiently rich for parameter estimation and validation of the integrated process model.

2. Materials and methods

2.1. Catalysts preparation and characterization

TiO_2 was used to prepare a catalytic film on a stainless steel sheet of 0.1 mm thickness as support following the method proposed by Lee et al. [37]. Before coating, the rectangle sheet of 0.157 m width (the sheet width matches with the perimeter of a circle of 0.05 m diameter) and 0.6 m length was washed with ethanol and dried at 80 °C for 15 min. 1.2 g of TiO_2 powder (P25 by Evonik; particle size of 21–30 nm; BET surface area of 50 m^2/g) was mixed with 0.4 g of acetyl acetone (Sigma-Aldrich). The mixture was added to a solution of 6.0 ml of deionized water and 0.24 g of polyethylene oxide (M.W. 1000, Sigma-Aldrich) and 0.24 g of polyethylene glycol (M.W. 8000, Sigma-Aldrich). Subsequently, the obtained paste was sonicated for 8 h and coated uniformly on the stainless steel sheet by a doctor blade method. The sheet coated with catalyst was annealed with air at 550 °C for 4 h. Finally, the catalytic sheet was rolled to form a cylinder and was placed on the inner wall of the reactor shell.

The phase change between the anatase and rutile crystal form of TiO_2 after annealing at 550 °C was investigated by X-ray diffraction (XRD) analysis (see Fig. S1 in the Supporting Information). The used TiO_2 is a combination of anatase (≈80%) and rutile (≈20%). The photocatalytic activity of anatase is superior to rutile [38]. It is well known that at high temperatures the anatase phase of TiO_2 converts to the rutile phase. Different temperatures have been reported for this transition [39]. Our XRD analysis showed that the anatase to rutile transition for P25 was negligible and reached only around 3% after being heated to 550 °C. The catalyst film thickness was measured by a profilometer (Dektak 8 Profiler, Veeco GmbH) at several locations on the catalytic sheet, which was found to be 25 ± 6 μm.

The fraction of photons reflected by the catalytic film was measured as function of wavelength using a spectroradiometer equipped with an integrating-sphere attachment (Perkin Elmer Lambda 900) with 150 mm integrating sphere. Fig. 1 shows the fraction of light reflected at different wavelengths of light. For the dominant wavelength used in this study (365 nm), the fraction of light reflected is 25%. Considering that there is no transmission of light in our catalytic system, the fraction of light absorbed is about 75%.

The fraction of light transmitted through the catalytic film and substrate material is assumed to be zero, because of the optically thick catalytic film and chosen substrate material [40]. Taking into account the closed and tubular reactor configuration and the possibility of re-absorption of reflected photons, any loss of photons due to reflection and subsequent absorption by any material other than the photocatalyst has been neglected when modelling the photocatalytic reactor. Therefore, any kinetic effects of photon reflection will be taken into account indirectly when fitting model parameters of reaction kinetics. In addition, the fraction of absorbed photons depends on the photon wavelength as depicted in Fig. 1. Therefore, for a polychromatic field, the monochromatic rate of photon absorption in the reaction kinetics is calculated by integration of photon absorption rates for different photon wavelengths over the catalytic surface. However, in this study due to the very narrow spectra of LEDs, the rate of photon absorption is approximated as a monochromatic radiation source of 365 nm wavelength.

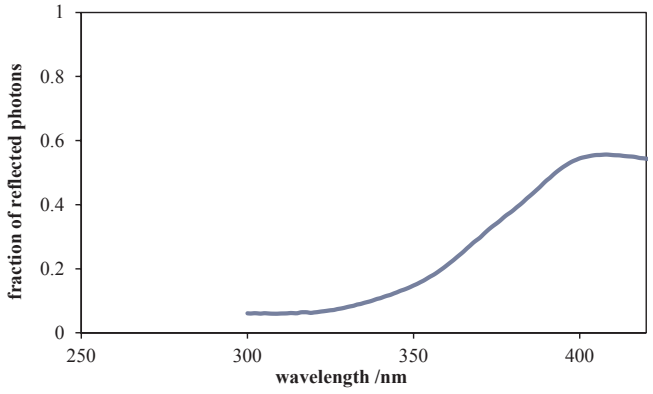

Fig. 1. Fraction of photons reflected by the catalytic sheet versus emitted photons wavelength.

2.2. Experimental set-up and method

A mini-pilot plant experimental set-up (Fig. 2) was designed and constructed. The set-up is composed of three main parts: a feed preparation system, a tubular LED-based photocatalytic reactor and a product sampling and analysis system.

The carrier gas in this study is a mixture representing air with N_2 (78%) and O_2 (22%). The reactor feed is generated by mixing three gas streams: a stream of carrier gas containing toluene, a humid stream of carrier gas with water vapour and a stream of carrier gas for dilution. Liquid toluene is used to generate toluene vapour in the carrier gas. First, regulated flows of pure N_2 and O_2 are mixed via two mass flow controllers (MFC) (F-201CV-1K0-RAD, Bronkhorst, the Netherlands) at a desired ratio to generate the carrier gas. The liquid toluene (anhydrous 99.8%, Sigma-Aldrich) is pressurized by helium in a stainless steel vessel of which the outlet flow is controlled by the MFC. The liquid toluene and the carrier gas flow into a Controlled Evaporator Mixer (E-7110-04-33-01-RAA, Bronkhorst, the Netherlands) where toluene is heated, vaporized and mixed with the carrier gas. A similar Controlled Evaporator Mixer system is used to obtain carrier gas humidified with water. The two carrier gas streams (toluene feed and humidified carrier gas) are mixed and further diluted with a third feed stream of carrier gas to provide the reactor feed of desired toluene concentration and relative humidity. Consequently, the initial toluene concentration and relative humidity of the resulting mixture can be varied in the range of 30–85 ppmv and 0–70%, respectively, before entering the reactor. The relative humidity of the feed is monitored at the reactor inlet and outlet using on-line thermohygrometers (model HC2-IE102, Rotronic). The photocatalytic degradation of toluene at the surface of a TiO_2 film is known to be more effective at room temperature rather than at elevated temperature [41]. Therefore, all experiments were performed at 30 °C. The reactor shell has a jacket through which water of 30 °C flows to keep the reactor temperature at this desired value. Furthermore, all of the conduits are made of stainless steel and are heat traced to keep the gas flow at 30 °C.

The standard configuration of the LED-based photocatalytic reactor consists of three concentric cylinders of the same length. The used UV-LEDs (NSSU100CT, Nichia, Japan) have a maximum spectral intensity at 365 nm and 10 nm half height width and a directivity of 55 °at 50% of irradiance. 246 LEDs are mounted evenly on the inner cylinder and distributed in such a way that they provide almost a uniform illumination pattern on the catalytic surface [23]. The irradiance emitted by the LEDs can be manipulated using current-control mode since irradiance of LEDs is linearly proportional to the applied current. Depending on the applied current, the power consumption of LEDs varied from 0.81 to 3.6 [W] in this study. The photon flux from the LEDs received by the catalytic film is measured by a calibrated spectroradiometer (Avaspec-ULS2048). The LEDs are separated from the reacting medium by a quartz cylinder in the middle, which is transparent to UV radiation. The outer cylinder is made of stainless steel and is used as the reactor shell to support the catalyst film. The catalytic sheet is placed on the inner wall of the reactor shell. A flow distributor with several small orifices is used at the reactor inlet to achieve a fully developed velocity profile at the cross section of the reactor. The system is characterized in terms of toluene conversion, mineralization, and catalyst deactivation for different reactor lengths and operational variables including toluene inlet concentration, relative humidity, volumetric

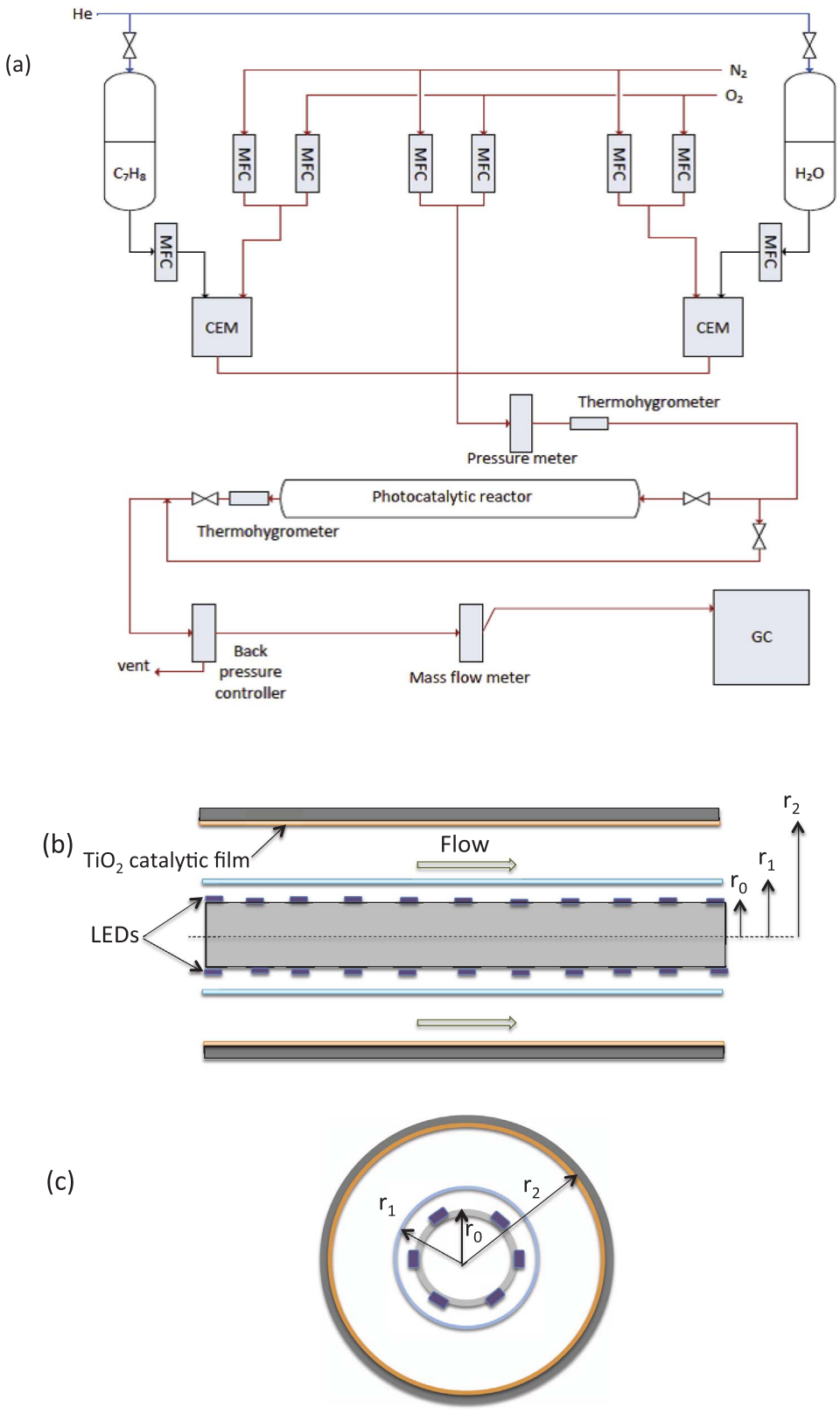

Fig. 2. (a) Schematic diagram of experimental set-up; (b) schematic reperesentation of the cross-sectional side view of the LED-photocatalytic reactor, and (c) schematic reperesentation of the cross-sectional view of the LED-photocatalytic reactor.

flow rate and irradiance. The experimental details including reactor geometry and operational conditions are summarized in Table 1. Every experiment in this study has been repeated at least once. The uncertainty of the experimental results has been reported as the 90% confidence interval.

A back pressure controller (P-702CV-6K0A-RAD, Bronkhorst, the Netherlands) keeps the reactor pressure at slightly above ambient pressure (1.09 bar) and the pressure of the system is measured using a pressure meter (P-502C-6K0A-RAD, Bronkhorst, the Netherlands) located before the reactor inlet. A part of the reactor effluent flows into an on-line Gas Chromatograph (GC) (GC-7890B, Agilent Technologies) with a constant flow rate, which is measured with a mass flow

Table 1
Reactor dimensions and operating conditions.

Photocatalytic reactor geometry		
L	reactor length [m]	0.12–0.6
r_0	LEDs tube radius [m]	0.008
r_1	quartz tube radius [m]	0.02
r_2	reactor shell radius [m]	0.025

Operation conditions

Experiment No.	Relative Humidity (RH) %	Irradiance (E) [W m^{-2}]	Toluene inlet concentration (C_{in}) [ppmv]	Volumetric flow rate (Q) [ml min^{-1}]
#1	40	13	19	1250
#2	40	13	30	1250
#3	40	13	42	1250
#4	40	13	52	1250
#5	40	13	70	1250
#6	40	13	80	1250
#7	40	13	42	500
#8	40	13	42	800
#9	40	13	42	1000
#10	40	13	42	1500
#11	0	13	42	800
#12	10	13	42	800
#13	25	13	42	800
#14	55	13	42	800
#15	70	13	42	800
#16	40	3	42	800
#17	40	5	42	800
#18	40	7	42	800
#19	40	9	42	800
#20	40	11	42	800

controller (F-201CV-1K0-RAD, Bronkhorst, the Netherlands). The remaining part of the reactor effluent flows into a vent. The GC is equipped with a methane convertor, two Flame Ionization Detectors (FID, one for hydrocarbons and another one for CO_2 concentrations lower than 50 ppm detection) and two Thermal Conductivity Detectors (TCD, one for N_2 and O_2 and another one for CO_2 detection). Gasses such as CO and CO_2 are separated with PPQ/Molseive columns. After the chromatographic separation has taken place, CO and CO_2 are converted to CH_4 using hydrogen on a nickel catalyst and measured as CH_4 with the FID detector. The advantage of using the FID detector is the much higher sensitivity and stability of FID compared to TCD. Although the GC configuration used in this study was designed and calibrated to detect a wide range of byproducts from photocatalytic degradation of toluene such as benzaldehyde and benzoic acid, no by-product was detected in the reactor effluent gas.

Before starting a catalytic test, the reactor feed is injected into the GC via a bypass line to analyse the feed composition. Subsequently, the reactor is purged for 2 h with feed without illumination to reach the equilibrium state. Finally, the illumination is started and the concentrations of the various species in the reactor effluent are measured every 20 min. All the experimental data are obtained using the same catalytic film to prevent any bias resulting from differences in catalyst surface and thickness. However, due to catalyst deactivation, the catalyst was regenerated rigorously before conducting a new experiment.

To investigate the catalyst deactivation, experiments are carried out for a period of 240 min. It has been reported that O_2 molecules are necessary for faster catalyst regeneration since the humidified N_2 stream cannot efficiently regenerate the catalyst activity [42]. Therefore, before every experiment, the photocatalyst is regenerated by using an 800 ml min^{-1} humidified air (55% RH) stream with 13 W m^{-2} of UV irradiance for 8 h. Only the first 30 min of every experiment have been considered to determine the steady state, because the catalyst activity decreased over longer periods for some experiments. Catalyst deactivation is not included in the steady-state process model described in the next section.

2.3. Reactor modelling and validation

The model used in this work and its assumptions have been described in detail elsewhere [23] and is summarized here for completeness including an extension to consider different effects of water on the reaction kinetics. The model is based on material, momentum and radiation balance equations. The internal mass transfer within the catalytic film has been neglected since the catalyst film is thin and non-porous. Biard et al. [43] found that the internal mass transfer is negligible for a similar system as used in this study, which justifies our assumption.

The toluene mole balance within the reactor is described by:

$$D\frac{1}{r}\frac{\partial}{\partial r}\left(r\frac{\partial C(r,z)}{\partial r}\right)-u(r)\frac{\partial C(r,z)}{\partial z}=0, \tag{1}$$

where the diffusion coefficient of toluene in air, D [m^2 s^{-1}] is 8.8×10^{-6} [19]. $C(r, z)$ [mol m^{-3}] is the toluene concentration as function of radial and axial direction and $u(r)$ [m s^{-1}] is the gas velocity profile for a fully developed laminar flow in an annulus described by:

$$u(r)=2\frac{Q}{\pi r_2^2}\frac{\ln\left(\frac{r_1}{r_2}\right)}{\left[\left(1-\left(\frac{r_1}{r_2}\right)^4\right)\ln\left(\frac{r_1}{r_2}\right)+\left(1-\left(\frac{r_1}{r_2}\right)^2\right)^2\right]}\left(1-\left(\frac{r}{r_2}\right)^2-\frac{\left[1-\left(\frac{r_1}{r_2}\right)^2\right]}{\ln\left(\frac{r_1}{r_2}\right)}\ln\left(\frac{r}{r_2}\right)\right), \tag{2}$$

where r_1 is the radius of the inner tube (quartz tube) and r_2 is the radius of the outer tube (reactor shell). Considering the fact that chemical reactions only occur on the catalytic surface, the boundary conditions for solving Eq. (1) are:

$$D\frac{\partial C(r_2,z)}{\partial r}=-R, \tag{3}$$

$$\frac{\partial C(r_1,z)}{\partial r}=0, \tag{4}$$

$$C(r,0)=C_{in}, \tag{5}$$

where C_{in} [mol m^{-3}] is the concentration of toluene at the reactor inlet and R [mol m^{-2} s^{-1}] is the toluene degradation rate. The Langmuir-Hinshelwood (L-H) mechanism has been widely applied to describe the reaction rate at the initial step of photocatalytic reaction [6,44,45] including the photocatalytic degradation rate of toluene [31,46]. Since the by-products and intermediates are normally formed in trace amounts and could not be detected at the reactor outlet during our experimental tests despite the used GC configuration that was calibrated to detect typical by-products from toluene degradation, their effects on the reaction rate are ignored:

$$R\propto\theta_t \tag{6}$$

where θ_t is the toluene coverage on the catalytic surface.

A photocatalytic reaction rate can often be described by a power law in association with the rate of photon absorption [47]. The details of the radiation field model of an array of LEDs are given elsewhere [23]. Furthermore, the radiation field model has been validated for the reactor used here in prior work [23]. The reaction rate is proportional to irradiance:

$$R\propto E^{\gamma}, \tag{7}$$

where the exponent γ has a value between 1 and 0, which can typically be estimated using non-linear data fitting. At low irradiance, the

reaction rate is proportional to irradiance since the limiting step is electron-hole generation. When further increasing the irradiance, the electron-hole generation rate surpasses the reactant consumption rate, stimulating charge recombination processes which causes a transition from a first order to a square root dependency with respect to irradiance. Finally, at the light-saturated regime, the reaction rate becomes independent of irradiance since the reaction is limited by mass transfer [7,48,49].

In several studies, photocatalytic degradation of toluene has been described successfully by a simple uni-molecular L-H, considering only toluene adsorption on the catalytic surface [13,28,31,46,50]:

$$R = -E^{\gamma}k\frac{KC_t}{1 + KC_t}, \tag{8}$$

where k and K are the rate constant and adsorption equilibrium constant, respectively. C_t is toluene concentrations on the catalyst surface. However, it may be needed to include the effect of water concentration in the reaction rate expression [32]. Humidity can play a significant role in a photocatalytic oxidation mechanism via transformation of water into hydroxyl radicals on the catalyst surface, which are highly reactive oxidants. In addition, water can also suppress electron-hole recombination [31]. On the other hand, the surface of TiO_2 is hydrophilic, which results in competitive adsorption between the reactants and water on the catalytic sites [29]. Consequently, increasing the water content may decrease toluene adsorption on TiO_2 active sites, affecting toluene coverage on the catalytic surface and, therefore, reaction rate. To better predict the effect of water on the process behaviour, a competitive bi-molecular L-H reaction rate model, described by

$$R = -E^{\gamma}k\frac{K_tC_t}{1 + K_wC_w + K_tC_t}, \tag{9}$$

is investigated as an alternative to simple L-H kinetics described by Eq. (8). In Eq. (9), K_t and K_w are the toluene and water adsorption equilibrium constant and C_w is the water concentration. Four series of experiments are conducted at identical operating conditions except for the toluene and water inlet concentrations, irradiances and volumetric flow rates (see Table 1) to compare the performance of both models for reaction kinetics within the overall process model when describing the experimental data.

When neglecting any volume changes for different toluene concentrations that have low values in this study, the average concentration of toluene ($C_{t,out,mod}$) at the reactor outlet and toluene conversion are given by:

$$C_{t,out,mod} = \frac{\int_{r_1}^{r_2} C_t(r,L)u(r)rdr}{\int_{r_1}^{r_2} u(r)rdr}, \tag{10}$$

$$\text{conversion} = 1 - \frac{C_{t,out}}{C_{t,in}} \tag{11}$$

where L is the reactor length and r_1 and r_2 are the inner and outer annulus radius. $C_{t,in}$ and $C_{t,out}$ are toluene concentrations at the reactor inlet and outlet. Toluene mineralization is defined as the ratio of toluene moles converted to form CO_2 to the total moles of toluene converted (complete oxidization of 1 mol toluene results in the formation of 7 mol of CO_2) and described as follows [28]:

$$\text{mineralization} = \frac{1}{7}\frac{\text{mole}_{CO_2,formed}}{\text{mole}_{toluene,converted}}. \tag{12}$$

The reactor model is solved using Matlab R2014b. An optimization algorithm is used for fitting the model parameters to experimental data by minimizing the following error function:

$$\text{error} = \sum_{i=1}^{N} (C_{t,out,exp}(i) - C_{t,out,mod}(i))^2, \tag{13}$$

where N is the number of data points obtained from multiple identical experiments and $C_{t,out,exp}$ and $C_{t,out,mod}$ are the toluene outlet concentrations from the experiments and the model, respectively.

The differential Eq. (1) is solved via discretization along the axial and radial directions using finite difference approximations. In particular, a first-order upwind scheme is used to produce $N_R \times N_L$ algebraic equation (where N_R is the number of grid points in the radial direction and N_L is the number of grid points in the axial direction), which are solved simultaneously.

3. Results and discussion

3.1. Model validation and parameter estimation

3.1.1. Mass transfer limitations

A number of experiments were conducted to study any mass transfer limitation in the reactor. Changing the volumetric feed flow rate will change both the residence time (τ) as well as the flow conditions inside the reactor when reactor length is constant. Therefore, for a fair comparison, a series of experiments were conducted at different volumetric flow rates, but with the same residence time, toluene inlet concentration, irradiance and RH. To be able to keep the residence time constant at different flow rates, the modular design of the reactor was used by controlling the illumination in each of the 5 identical modules of 0.12 [m] in length independently. Considering the fact that there is no photocatalytic reaction at darkness, it is possible to vary the reaction length by either switching on or off the LED arrays in each module. Any boundary effects between illuminated and dark modules have been neglected. In particular, since the catalyst receives light from multiple sources, a sharp transition from illuminated to dark conditions between neighboring modules cannot be accomplished in practice. However, such boundary effects are expected to be small due to the high aspect ratio of the reactor. The results show that the volumetric flow rate has no significant influence on the toluene conversion at different volumetric flow rates (Fig. 3). Therefore, it can be concluded that at least under the operating conditions applied in this study, mass transfer limitations are small compared to limitations in reaction rate. In case volumetric flow rates would become much higher compared to the values applied in this study, our assumption of a fully developed laminar flow would be violated. In such case, a film model should be used to describe the mass transfer in the system.

3.1.2. Kinetic model

The integrated process model describes the toluene conversion reasonably well (see Fig. S2(a) in SI for the parity plot) when using a simple uni-molecular L-H reaction rate equation (Eq. (8)) at a fixed RH of 40% after parameter estimation. However, the model with uni-molecular L-H kinetics failed to describe the toluene conversion when parameter estimation was based on the full data set including experiments at different RH, which was indicated by an error function value that was about 5 times higher compared to the case at constant RH (see Fig. S2(b) in SI for the parity plot). The estimated parameter values and error function values for both cases are given in Table 2. It is clear that the influence of water should be included in the reaction rate equation to describe the experimental data well.

The estimated parameters and error function value for the model including Eq. (9) are also reported in Table 2 (see Fig. S3 in supporting information for the parity plot). It can be seen that the competitive bi-molecular L-H reaction rate explains the experimental data satisfactorily in the studied range for all experiments. Therefore, it is concluded that for varying water concentrations, the competitive bi-molecular L-H reaction rate offers a more suitable description of the system behaviour. The reaction rate can be simplified to the simple uni-molecular L-H only if the water concentration does not change, which would simplify modeling and optimization.

The estimated parameters in this work are comparable to the values reported by others for a system with a similar catalyst, operating

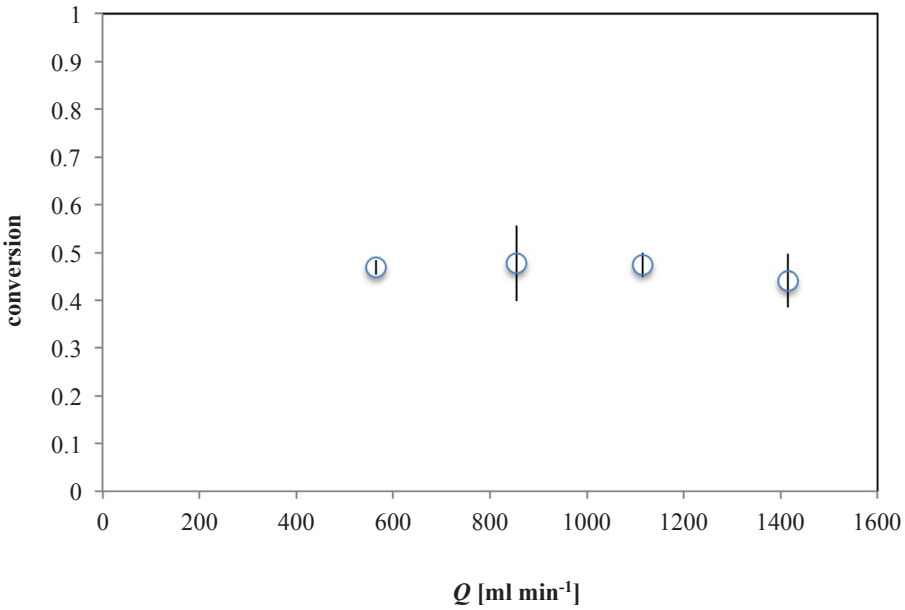

Fig. 3. Toluene photocatalytic conversion versus volumetric flow rate for Cin ≈ 29 ppmv, τ = 18 s, E = 13 Wm^{-2} and RH = 40%.

conditions and reaction rate expression [51]. However, different values for the kinetic parameters have been reported as well for other systems [32,52]. Although the parameter values are still within the same order of magnitude, such comparison shows that differences in catalyst properties, reactor system, operating conditions, and expression for the reaction rate can lead to different values for the kinetic parameters compared to the ones estimated in this work.

3.2. Experimental characterization of reactor performance

No degradation of toluene was found under either dark conditions or in absence of catalyst. Carbon dioxide was the main product of the photocatalytic experiments and no intermediates or by-products other than a trace amount of benzene (≈0.2 ppm) were identified by GC/FID. In case of complete oxidization of toluene to carbon dioxide, it is expected that 7 mol of carbon dioxide are formed per mole of toluene converted. However, a carbon balance showed only a partial oxidation of toluene to carbon dioxide, which varied from 22 to 87% depending on the operating conditions. By-products could have been adsorbed on the catalytic surface, as it has been reported by other researchers as well [29], or remained undetected in the GC/FID analysis. Adsorption of by-products is most likely since catalyst deactivation was observed for several experiments.

3.2.1. The effect of toluene and water inlet concentration

The effect of toluene inlet concentration on the toluene conversion and mineralization to CO_2 is shown in Fig. 4. It can be seen that both toluene conversion and mineralization decrease by increasing toluene inlet concentration, which may be explained by the toluene degradation kinetics according to a L-H mechanism. When increasing the toluene inlet concentration, although the reaction rate is expected to increase, conversion decreases (see Eqs. (9) and (11)). The toluene degradation could be limited by the number of catalyst active sites [39,45]. In addition, increasing the toluene inlet concentration may result in a more dominant role of mass transfer compared to photon transfer. The reason

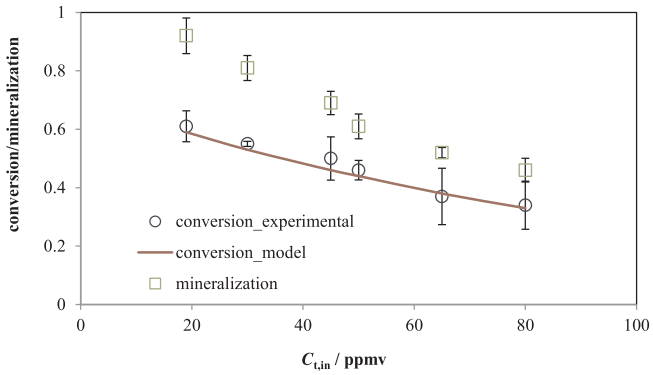

Fig. 4. Effect of toluene inlet concentration on the conversion and mineralization of toluene for Q = 1270 ml min^{-1}, E = 13 W m^{-2}, RH = 40% (see Table 1). Error bars indicate the 90% confidence interval.

Table 2
Kinetic and adsorption equilibrium parameters obtained from parameter estimation when using the reaction rate expressions (8) and (9) in the reactor model including objective function value (err) of the found minimum.

Rate expression	Parameters	Values	Units	Err	Remark
$R = -E^{\gamma} k \frac{KC_t}{1+KC_t}$ (8)	k	1.64×10^{-7}	mol m^{-1} s^{-1} $W^{-0.5}$	0.0014	For the experimental results at fixed RH of 40%
	K	692	m^3 mol^{-1}		
	γ	0.5	–		
$R = -E^{\gamma} k \frac{KC_t}{1+KC_t}$ (8)	k	8.9×10^{-8}		0.0060	For all the experimental results including all tested water concentrations
	K	1160			
	γ	0.5			
$R = -E^{\gamma} k \frac{K_t C_t}{1+K_w C_w + K_t C_t}$ (9)	k	1.04×10^{-7}	mol m^{-1} s^{-1} $W^{-0.5}$	0.0027	For all the experimental results including all tested water concentrations
	K_t	2089	m^3 mol^{-1}		
	K_w	3.32	m^3 mol^{-1}		
	γ	0.5	–		

is that the number of toluene molecules adsorbed on the catalytic surface surpasses the number of generated electron-hole pairs by photon absorption on the catalytic surface. As a result, the electron-hole pairs on the catalytic surface may become insufficient to initiate a chemical reaction with the adsorbed reactants. Thus, photon delivery from the light source to the catalytic surface and subsequent charge generation becomes the reaction controlling factor.

According to Eq. (9), by increasing the toluene concentration at the inlet, although the fractional conversion decreases, the absolute number of moles of toluene that are converted increases. However, the number of CO_2 moles formed remains almost constant by varying toluene inlet concentration. Therefore, according to Eq. (12), toluene mineralization decreases when increasing the toluene inlet concentration. This decreasing mineralization can be attributed to the fact that at the very first step, toluene is converted to intermediates. In the next steps, the intermediates undergo subsequent surface reactions producing the final product (CO_2), which is apparently not affected by the toluene inlet concentration but possibly by other factors such as water concentration. In fact, at a fixed molar flow of water, the number of moles of CO_2 formed remains constant, which results in a decrease in mineralization when the toluene feed molar flow rate increases. Therefore, it is concluded that CO_2 formation mainly depends on the water molar flow rate.

To investigate the effect of the water content in the feed on the photocatalytic degradation of toluene, experiments were carried out at different relative humidity values. The maximum conversion was obtained at low water concentrations (Fig. 5), which is in agreement with some studies [28,29] and in contrast to other studies where no toluene degradation was reported in the absence of water [30–34]. Different reaction paths have been suggested for toluene degradation on UV-illuminated TiO_2 [28,35,53]. d'Hennezel et al. [35] proposed that the OH radical is not the dominant reactive agent in gas phase photocatalytic oxidation of many volatile organic compounds (VOCs) including toluene, which can explain the high conversion at no or very low water concentrations in the present study. When increasing the water content, conversion decreases gradually which can be caused by the competition between water and toluene adsorption on the catalyst active sites as it has been expressed in the reaction rate (Eq. (9)) that gave the best model fit to our data.

In contrast to toluene conversion, mineralization increased significantly by increasing the water content of the feed (Fig. 5), which can be explained by the involved reaction steps. Toluene conversion is determined by the initial step of the degradation reaction sequence where mass and photon transfer to the catalytic surface and the availability of catalyst active sites are dominant factors in contrast to relative humidity and hydroxyl radicals, which may play minor roles. On the other hand, the role of hydroxyl radicals becomes possibly more dominant when converting intermediates, formed in initial step of degradation, to

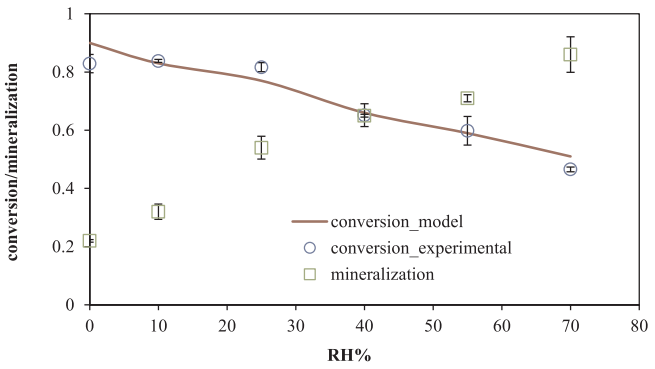

Fig. 5. Effect of relative humidity on the conversion and mineralization of toluene for $C_{in} \approx 45$ ppmv, $Q = 812$ ml min^{-1} and $E = 13$ W m^{-2}. Error bars indicate the 90% confidence interval.

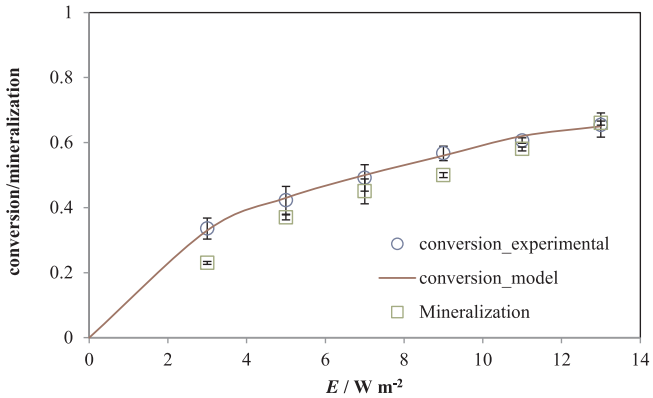

Fig. 6. Effect of the average irradiance on the toluene conversion for Cin ≈ 45 ppmv, Q = 800 ml min^{-1} and RH = 40%,. Error bars indicate the 90% confidence interval.

CO_2 for our experimental conditions. Consequently, by increasing the water content in the feed, the number of hydroxyl radicals on the catalytic surface increases leading to increased toluene mineralization.

3.2.2. The effect of irradiance

The effect of irradiance on the toluene conversion and mineralization is illustrated in Fig. 6 in the range of 0–13 W m^{-2}. It can be seen that by increasing irradiance, the toluene conversion increases approximately by the square root of the irradiance for all tested irradiance levels, which implies that the rate of photon transfer surpasses the rate of mass transfer leading to charge recombination. Furthermore, when increasing the irradiance, mineralization increases. The electron-hole pairs generated on the catalytic surface may either react with water to form hydroxyl radicals needed for mineralization or directly with adsorbed intermediates on the catalyst surface which both can enhance CO_2 formation and thus mineralization. In terms of energy consumption, the LED-based reactor is able to convert 0.15–0.80 mol of toluene per KW consumed depending on the operating conditions.

3.2.3. The effect of residence time

The effect of residence time in the range of 16–50 s (corresponding to volumetric flow rates of 500–1500 ml min^{-1}) on the toluene conversion and mineralization is shown in Fig. 7. An increase in volumetric flow rate, and consequently a decrease in residence time, results in a conversion drop as it was observed in other studies as well [28,54]. For a surface catalytic reaction, a decrease in contact time between reactants and a catalytic surface should result in a conversion drop. In addition, toluene binds relatively weak with TiO_2, suggesting enhanced effectiveness of contact time on the reactor performance [28]. As demonstrated earlier, changes in the volumetric feed flow rate at constant contact time do not improve the mass transfer of reactant from the bulk

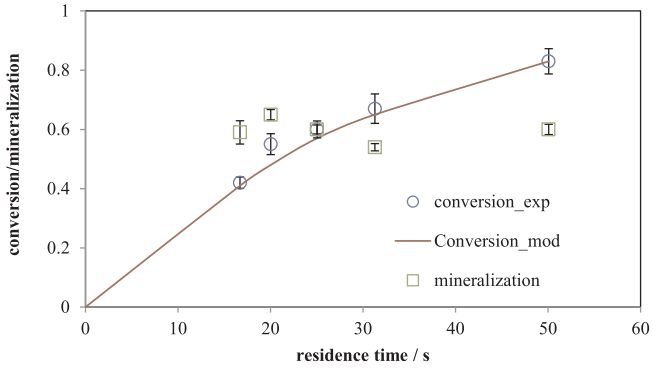

Fig. 7. Effect of residence time (derived from volumetric flow rate and reactor volume) on the toluene conversion and mineralization for Cin ≈ 45 ppmv, RH = 40%, E = 13 W m^{-2}. Error bars indicate the 90% confidence interval.

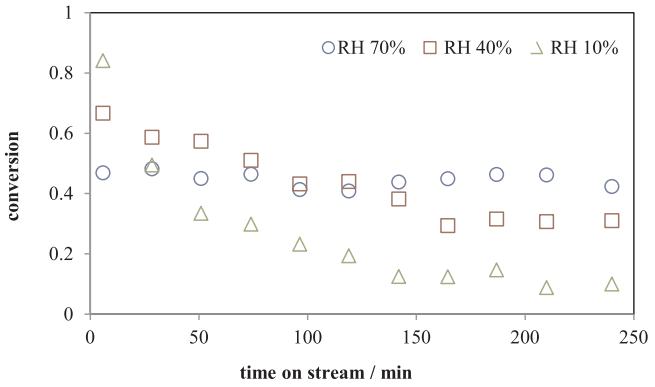

Fig. 8. Toluene conversion versus time for three different relative humidity values for Cin ≈ 45 ppmv, Q = 812 ml min^{-1} and E = 13 W m^{-2}.

to the catalytic surface significantly. Furthermore, the integrated process model, which does not include enhanced mass transfer at higher flow rates, describes the experimental data well. Therefore, it is concluded that the contact time between catalyst and reactant is the most dominant factor for the conditions studied in this work.

Toluene mineralization remains essentially unchanged when varying the volumetric flow rate and, consequently, the residence time. A possible reason for this observation is the fixed toluene to water molar ratio for these experiments. As discussed above, toluene conversion is a function of contact time and mass transfer for which volumetric flow rate plays a significant role. However, CO_2 is a product of multiple surface reaction steps involving various intermediates [28,35]. The OH radicals are an important oxidation agent to achieve full mineralization. Therefore, the number of CO_2 moles formed to the number of toluene moles converted may remain constant at a fixed toluene to water molar ratio.

3.3. Catalyst deactivation and regeneration

Catalyst activity dropped under various operating conditions over the course of several hours (Fig. 8). This catalyst deactivation is most likely caused by partial oxidation of toluene to intermediates, which can accumulate on the catalyst surface when time progresses [55]. Larson et al. [56] found that toluene is converted to less-reactive intermediates in the initial step of degradation, which make stronger bonds to TiO_2 compared to toluene. Thus, those intermediates may block the catalyst active sites, which inhibits adsorption of toluene molecules and deactivates the catalyst.

The effects of relative humidity and toluene inlet concentration on the catalyst deactivation are shown in Fig. 9. It can be seen that water plays a significant role in maintaining catalyst activity (Fig. 9(a)). Most probably, hydroxyl radicals formed after water adsorption on the TiO_2 active sites react with strongly adsorbed intermediates, which release from the catalyst surface in the form of CO_2. As a result, mineralization enhances while the catalyst maintains its activity as discussed before. At the lowest tested toluene concentration (19 ppmv) no catalyst deactivation was observed at a fixed relative humidity of 40% while toluene degradation reduced to less than half after 4 h of operation when increasing the toluene inlet concentration to 30 ppmv. Upon further increasing the toluene inlet concentration to 80 ppmv, a slight decrease in toluene degradation can be observed (Fig. 9(b)). A higher toluene inlet concentration results in a higher number of toluene moles converted to intermediates. Therefore, the required water content to prevent significant catalyst deactivation is correlated to the toluene inlet concentration. However, it can be seen that after a certain toluene concentration, the rate of catalyst deactivation becomes less sensitive to the toluene inlet concentration, which may be explained by saturation of the catalyst surface. No significant trend in the rate of catalyst deactivation was observed by changing irradiance or residence time at fixed

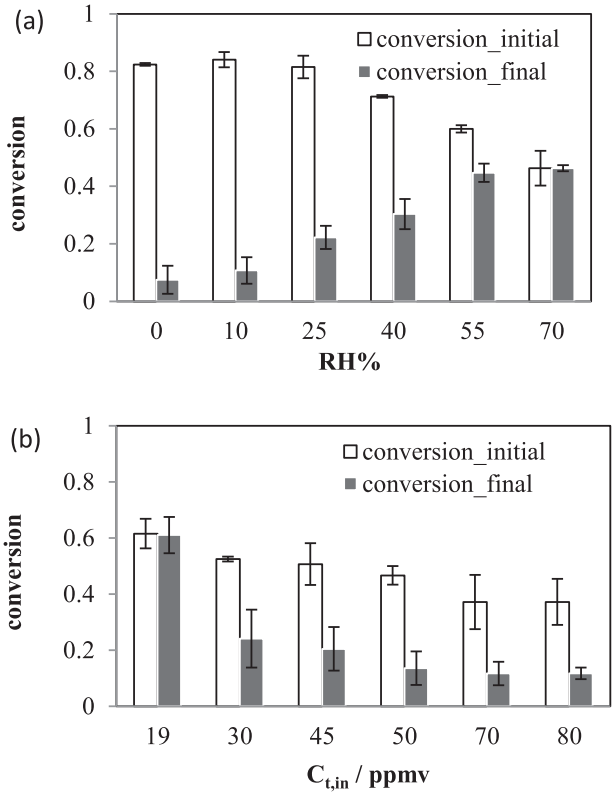

Fig. 9. Initial (after 6 min) and final (after 4 h) conversion as a function of (a) relative humidity (C_{in} ≈ 45 ppmv, Q = 812 ml min^{-1} and E = 13 W m^{-2}) and (b) toluene inlet concentration (RH = 40%, Q = 1270 ml min^{-1} and E = 13 Wm^{-2}). Error bars indicate the 90% confidence interval.

water to toluene molar flow ratio (data not shown).

To better predict the effect of water on catalyst activity, the rate of change of the toluene conversion over time (d*X*/dt) as function of relative humidity is shown in Fig. 10. It can be seen that the rate of catalyst deactivation decreases linearly with RH. Furthermore, the rate of catalyst deactivation was relatively low compared to the other dynamics of the system. Therefore, a correction factor as a function of relative humidity could be included in the process model to predict the rate of catalyst deactivation under pseudo steady–state conditions.

Finally, to test the regeneration of the catalyst, the toluene outlet concentrations versus time for three experiments with identical conditions for the same catalyst are compared in Fig. 11. The three experiments show very comparable results. Therefore, it is concluded that, although catalyst deactivation clearly occurs for certain experiments, full recovery of catalyst activity is obtained after applying the regeneration process described in Section 2.2. At the first minutes of the regeneration process, typically a high concentration of CO_2 is detected in the reactor effluent, which decreases by time as the catalyst regeneration proceeds until no CO_2 is detected after 6–8 h indicating full recovery of catalyst activity.

4. Conclusion

An integrated process model describing an annular LED-based photocatalytic reactor including a radiation field model from LEDs, reaction kinetics, and mass transfer is successfully validated experimentally for a broad range of operating conditions. A special focus is on the role of water. Parameter estimation based on experimental data demonstrates that including competitive water adsorption enhances model prediction significantly compared to simple uni-molecular Langmuir-Hinshelwood kinetics.

Experimental characterization of a mini-pilot plant setup shows that

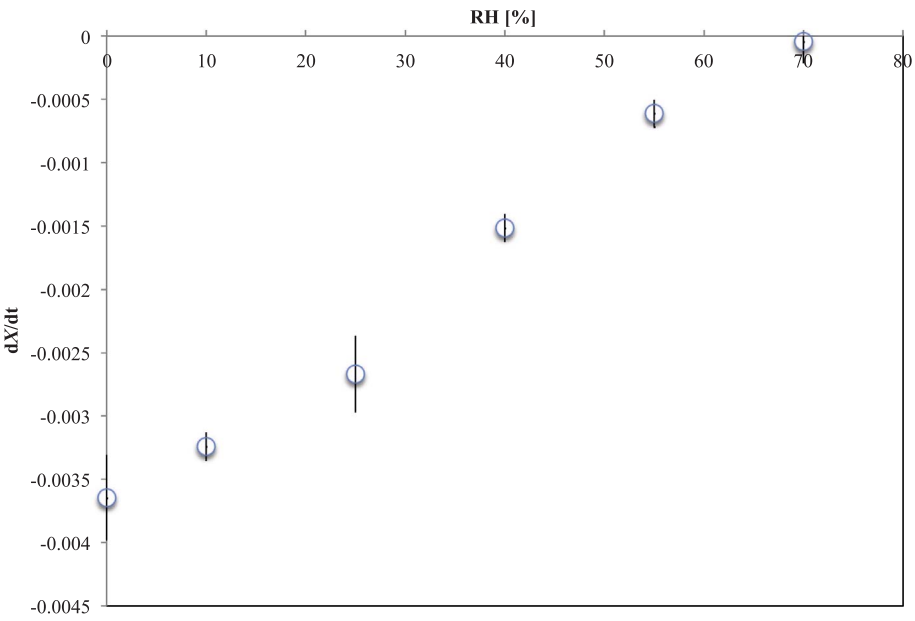

Fig. 10. The rate of catalyst deactivation vs. RH%.

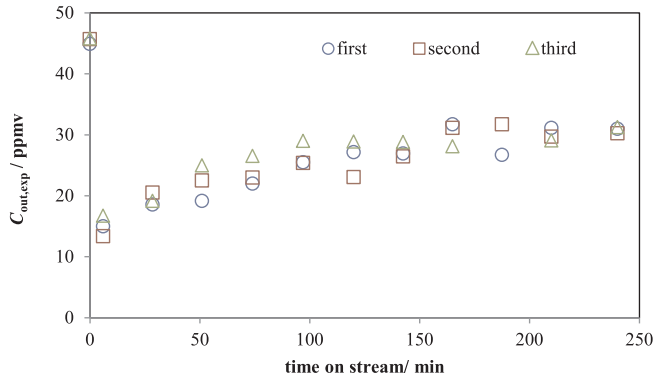

Fig. 11. Toluene outlet concentrations for three experiments with identical conditions (Cin ≈ 45 ppmv, RH = 40%, Q = 812 ml min^{-1} and E = 13 W m^{-2}).

a rise in toluene inlet concentration from 19 to 80 ppmv results in a decrease of toluene conversion, which is likely caused by an increasing mass transfer rate as opposed to the photon transfer rate. In the absence of water or at very low water concentrations, toluene conversion is maximized indicating a limited role of water in the first step of toluene degradation. Toluene conversion decreases gradually when increasing the relative humidity to 70%, which can be caused by the competition among toluene and water for adsorption on the catalyst active sites. Furthermore, toluene degradation varies by the square root of irradiance when increasing irradiance from 3 to 13 W m^{-2}. Thus, it can be concluded that mass transfer resistant becomes dominant, leading to charge recombination for the studied operating conditions. Increasing the volumetric flow rate of the feed from 500 to 1500 ml min^{-1} results in a decrease in toluene conversion due to a decrease of the reactants and catalyst contact time.

Toluene mineralization to CO_2 is a strong function of the ratio of water to toluene molar flow rate. Toluene mineralization decreases when increasing the toluene inlet concentration or when decreasing the ratio of water to toluene molar flow rates. Therefore, it is concluded that hydroxyl radicals originating from water are the dominant species for conversion of reaction intermediates to CO_2. At fixed water to toluene molar flow, an increase in irradiance enhances toluene mineralization which can be explained by an increase in the formation of hydroxyl radicals from the increased irradiance. On the other hand, at a fixed toluene to water molar flow rate and irradiance, mineralization remains constant when changing the volumetric flow rate.

For conditions with low relative humidity, significant catalyst deactivation occurred over time, which was likely due to strong adsorption of reaction intermediates on the catalyst active site. Relative humidity plays an important role in the reaction of the intermediates, releasing them in the form of CO_2 from the catalyst surface and maintaining catalyst activity. Full recovery of the catalyst activity can be achieved by using humidified air in the presence of UV-illumination for 6–8 h.

Even though the integrated model of a LED-based photocatalytic reactor was successfully validated by this experimental study under fully developed laminar flow condition, the practical limitation of the experimental set-up hindered the investigation of the effect of volumetric flow rates higher than 1500 ml/min. However, higher volumetric flow rates may be applied for certain practical cases, where different mass transfer mechanisms may play a role due to the change in flow regime. Therefore, future works should focus on the effect of higher volumetric flow rates and the required model modification to account for the different flow regime and mass transfer mechanism.

Acknowledgments

This research is funded from the European Research Council in the framework of the Seventh Framework Programme (FP7) under grant agreement no ERC-2010-AdG-267348. Ruud Hendrix from the Department of Materials Science and Engineering of the Delft University of Technology is acknowledged for support with the X-ray analysis.

Appendix A. Supplementary data

Supplementary data associated with this article can be found, in the online version, at http://dx.doi.org/10.1016/j.cej.2017.09.108.

References

[1] A.F. Tooru Inoue, Satoshi Konishi, Kenichi Honda, Photoelectrocatalytic reduction of carbon dioxide in aqueus suspension of semiconductor powders, Nature 277 (1979) 2.
[2] S. Banerjee, D.D. Dionysiou, S.C. Pillai, Self-cleaning applications of TiO2 by photo-induced hydrophilicity and photocatalysis, Appl. Catal. B 176–177 (2015) 396–428.
[3] C. Hu, Y. Lan, J. Qu, X. Hu, A. Wang, Ag/AgBr/TiO2 visible light photocatalyst for destruction of azodyes and bacteria, J. Phys. Chem. B 110 (2006) 4066–4072.
[4] G. Marcì, M. Addamo, V. Augugliaro, S. Coluccia, E. Garcìa-López, V. Loddo,

G. Martra, L. Palmisano, M. Schiavello, Photocatalytic oxidation of toluene on irradiated TiO2: comparison of degradation performance in humidified air, in water and in water containing a zwitterionic surfactant, J. Photochem. Photobiol. A: Chem. 160 (2003) 105–114.
[5] A. Fujishima, K. Honda, Electrochemical photolysis of water at a semiconductor electrode, Nature 238 (1972) 37–38.
[6] M.A. Fox, M.T. Dulay, Heterogeneous photocatalysis, Chem. Rev. 93 (1993) 341–357.
[7] D.F. Ollis, E. Pelizzetti, N. Serpone, Photocatalyzed destruction of water contaminants, Environ. Sci. Technol. 25 (1991) 1522–1529.
[8] M.R. Hoffmann, S.T. Martin, W. Choi, D.W. Bahnemann, Environmental applications of semiconductor photocatalysis, Chem. Rev. 95 (1995) 69–96.
[9] J. Zhao, X. Yang, Photocatalytic oxidation for indoor air purification: a literature review, Build. Environ. 38 (2003) 645–654.
[10] T. Van Gerven, G. Mul, J. Moulijn, A. Stankiewicz, A review of intensification of photocatalytic processes, Chem. Eng. Process. 46 (2007) 781–789.
[11] R. Lakerveld, G.S.J. Sturm, A.I. Stankiewicz, G.D. Stefanidis, Integrated design of microwave and photocatalytic reactors. Where are we now? Curr. Opin. Chem. Eng. 5 (2014) 37–41.
[12] M. Motegh, J.R. van Ommen, P.W. Appel, M.T. Kreutzer, Scale-up study of a multiphase photocatalytic reactor–degradation of cyanide in water over TiO2, Environ. Sci. Technol. 48 (2014) 1574–1581.
[13] V. Tomasic, F. Jovic, Z. Gomzi, Photocatalytic oxidation of toluene in the gas phase: Modelling an annular photocatalytic reactor, Catal. Today 137 (2008) 350–356.
[14] F.V.S. Lopes, S.M. Miranda, R.A.R. Monteiro, S.D.S. Martins, A.M.T. Silva, J.L. Faria, R.A.R. Boaventura, V.J.P. Vilar, Perchloroethylene gas-phase degradation over titania-coated transparent monoliths, Appl. Catal. B 140–141 (2013) 444–456.
[15] A.E. Cassano, C.A. Martin, R.J. Brandi, O.M. Alfano, Photoreactor analysis and design – fundamentals and applications, Ind. Eng. Chem. Res. 34 (1995) 2155–2201.
[16] G.E. Imoberdorf, A.E. Cassano, O.M. Alfano, H.A. Irazoqui, Modeling of a multiannular photocatalytic reactor for perchloroethylene degradation in air, AlChE J. 52 (2006) 1814–1823.
[17] M.M. Hossain, G.B. Raupp, S.O. Hay, T.N. Obee, Three-dimensional developing flow model for photocatalytic monolith reactors, AlChE J. 45 (1999) 1309–1321.
[18] M. Moazzem Hossain, G.B. Raupp, Radiation field modeling in a photocatalytic monolith reactor, Chem. Eng. Sci. 53 (1998) 3771–3780.
[19] M.J. Munoz-Batista, A. Kubacka, M.N. Gomez-Cerezo, D. Tudela, M. Fernandez-Garcia, Sunlight-driven toluene photo-elimination using CeO2-TiO2 composite systems: a kinetic study, Appl. Catal. B 140 (2013) 626–635.
[20] W.-K. Jo, R.J. Tayade, New generation energy-efficient light source for photocatalysis: LEDs for environmental applications, Ind. Eng. Chem. Res. 53 (2014) 2073–2084.
[21] D.H. Chen, X. Ye, K. Li, Oxidation of PCE with a UV LED photocatalytic reactor, Chem. Eng. Technol. 28 (2005) 95–97.
[22] T.S.N. Kalithasan Natarajan, H.C. Bajaj, Rajesh J. Tayade, Photocatalytic reactor based on UV-LED/TiO2 coated quartz tube for degradation of dyes, Chem. Eng. J. 178 (2011) 40–49.
[23] F. Khodadadian, A. Poursaeidesfahani, Z. Li, J.R. van Ommen, A.I. Stankiewicz, R. Lakerveld, Model-based optimization of a photocatalytic reactor with light-emitting diodes, Chem. Eng. Technol. 39 (2016) 1946–1954.
[24] Z. Wang, J. Liu, Y. Dai, W. Dong, S. Zhang, J. Chen, CFD modeling of a UV-LED photocatalytic odor abatement process in a continuous reactor, J. Hazard. Mater. 215–216 (2012) 25–31.
[25] Z. Pengyi, L. Fuyan, Y. Gang, C. Qing, Z. Wanpeng, A comparative study on decomposition of gaseous toluene by O3/UV, TiO2/UV and O3/TiO2/UV, J. Photochem. Photobiol. A: Chem. 156 (2003) 189–194.
[26] Y.-P. Zhang, R. Yang, Q.-J. Xu, J.-H. Mo, Characteristics of photocatalytic oxidation of toluene, benzene, and their mixture, J. Air Waste Manage. Assoc. 57 (2007) 94–101.
[27] P.C. Yao, S.T. Hang, C.W. Lin, D.H. Hai, Photocatalytic destruction of gaseous toluene by porphyrin-sensitized TiO2 thin films, J. Taiwan Inst. Chem. Eng. 42 (2011) 470–479.
[28] M. Sleiman, P. Conchon, C. Ferronato, J.M. Chovelon, Photocatalytic oxidation of toluene at indoor air levels (ppbv): towards a better assessment of conversion, reaction intermediates and mineralization, Appl. Catal. B 86 (2009) 159–165.
[29] L.X. Cao, Z. Gao, S.L. Suib, T.N. Obee, S.O. Hay, J.D. Freihaut, Photocatalytic oxidation of toluene on nanoscale TiO(2) catalysts: studies of deactivation and regeneration, J. Catal. 196 (2000) 253–261.
[30] Y. Luo, D.F. Ollis, Heterogeneous photocatalytic oxidation of trichloroethylene and toluene mixtures in air: kinetic promotion and inhibition, time-dependent catalyst activity, J. Catal. 163 (1996) 1–11.
[31] S.B. Kim, S.C. Hong, Kinetic study for photocatalytic degradation of volatile organic compounds in air using thin film TiO2 photocatalyst, Appl. Catal. B 35 (2002) 305–315.
[32] C.A. Korologos, C.J. Philippopoulos, S.G. Poulopoulos, The effect of water presence on the photocatalytic oxidation of benzene, toluene, ethylbenzene and m-xylene in the gas-phase, Atmos. Environ. 45 (2011) 7089–7095.
[33] T.N. Obee, R.T. Brown, TiO2 photocatalysis for indoor air applications: effects of humidity and trace contaminant levels on the oxidation rates of formaldehyde, toluene, and 1,3-butadiene, Environ. Sci. Technol. 29 (1995) 1223–1231.
[34] T. Ibusuki, K. Takeuchi, Toluene oxidation on u.v.-irradiated titanium dioxide with and without O2, NO2 OR H2O at ambient temperature, Atmos. Environ. 20 (1986) 1711–1715.
[35] O. d'Hennezel, P. Pichat, D.F. Ollis, Benzene and toluene gas-phase photocatalytic degradation over H2O and HCL pretreated TiO2: by-products and mechanisms, J. Photochem. Photobiol. A: Chem. 118 (1998) 197–204.
[36] T. Guo, Z. Bai, C. Wu, T. Zhu, Influence of relative humidity on the photocatalytic oxidation (PCO) of toluene by TiO2 loaded on activated carbon fibers: PCO rate and intermediates accumulation, Appl. Catal. B 79 (2008) 171–178.
[37] D.M. Lee, H.J. Yun, S. Yu, S.J. Yun, S.Y. Lee, S.H. Mang, J. Yi, Design of an efficient photocatalytic reactor for the decomposition of gaseous organic contaminants in air, Chem. Eng. J. 187 (2012) 203–209.
[38] A. Sclafani, J.M. Herrmann, Comparison of the photoelectronic and photocatalytic activities of various anatase and rutile forms of titania in pure liquid organic phases and in aqueous solutions, J. Phys. Chem. 100 (1996) 13655–13661.
[39] D.A. Hanaor, C.C. Sorrell, Review of the anatase to rutile phase transformation, J. Mater. Sci. 46 (2011) 855–874.
[40] N. Padoin, C. Soares, An explicit correlation for optimal TiO2 film thickness in immobilized photocatalytic reaction systems, Chem. Eng. J. 310 (Part 2) (2017) 381–388.
[41] S.B. Kim, W.S. Cha, S.C. Hong, Photocatalytic degradation of gas-phase methanol and toluene using thin-film TiO2 photocatalyst II. Kinetic study for the effect of initial concentration and photon flux, J. Ind. Eng. Chem. 8 (2002) 162–167.
[42] J. Jeong, K. Sekiguchi, K. Sakamoto, Photochemical and photocatalytic degradation of gaseous toluene using short-wavelength UV irradiation with TiO2 catalyst: comparison of three UV sources, Chemosphere 57 (2004) 663–671.
[43] P.-F. Biard, A. Bouzaza, D. Wolbert, Photocatalytic degradation of two volatile fatty acids in an annular plug-flow reactor; kinetic modeling and contribution of mass transfer rate, Environ. Sci. Technol. 41 (2007) 2908–2914.
[44] J.-M. Herrmann, Photocatalysis fundamentals revisited to avoid several misconceptions, Appl. Catal. B 99 (2010) 461–468.
[45] C.S. Turchi, D.F. Ollis, Photocatalytic degradation of organic water contaminants: mechanisms involving hydroxyl radical attack, J. Catal. 122 (1990) 178–192.
[46] A. Bouzaza, C. Vallet, A. Laplanche, Photocatalytic degradation of some VOCs in the gas phase using an annular flow reactor – determination of the contribution of mass transfer and chemical reaction steps in the photodegradation process, J. Photochem. Photobiol. A Chem. 177 (2006) 212–217.
[47] M. Motegh, J.J. Cen, P.W. Appel, J.R. van Ommen, M.T. Kreutzer, Photocatalytic-reactor efficiencies and simplified expressions to assess their relevance in kinetic experiments, Chem. Eng. J. 207 (2012) 607–615.
[48] J.C. D'Oliveira, G. Al-Sayyed, P. Pichat, Photodegradation of 2- and 3-chlorophenol in titanium dioxide aqueous suspensions, Environ. Sci. Technol. 24 (1990) 990–996.
[49] Z.M. Wang, J. Liu, Y.C. Dai, W.Y. Dong, S.C. Zhang, J.M. Chen, Dimethyl sulfide photocatalytic degradation in a light-emitting-diode continuous reactor: kinetic and mechanistic study, Ind. Eng. Chem. Res. 50 (2011) 7977–7984.
[50] R.M. Alberici, W.F. Jardim, Photocatalytic destruction of VOCs in the gas-phase using titanium dioxide, Appl. Catal. B 14 (1997) 55–68.
[51] C. Passalía, O.M. Alfano, R.J. Brandi, Modeling and experimental verification of a corrugated plate photocatalytic reactor using computational fluid dynamics, Ind. Eng. Chem. Res. 50 (2011) 9077–9086.
[52] M.J. Muñoz-Batista, A. Kubacka, M. Fernández-García, Effective enhancement of TiO2 photocatalysis by synergistic interaction of surface species: from promoters to co-catalysts, ACS Catal. 4 (2014) 4277–4288.
[53] F. Zhang, X. Zhu, J. Ding, Z. Qi, M. Wang, S. Sun, J. Bao, C. Gao, Mechanism study of photocatalytic degradation of gaseous toluene on TiO2 with weak-bond adsorption analysis using in situ far infrared spectroscopy, Catal. Lett. 144 (2014) 995–1000.
[54] J. Jeong, K. Sekiguchi, W. Lee, K. Sakamoto, Photodegradation of gaseous volatile organic compounds (VOCs) using TiO2 photoirradiated by an ozone-producing UV lamp: decomposition characteristics, identification of by-products and water-soluble organic intermediates, J. Photochem. Photobiol. A: Chem. 169 (2005) 279–287.
[55] R. Méndez-Román, N. Cardona-Martínez, Relationship between the formation of surface species and catalyst deactivation during the gas-phase photocatalytic oxidation of toluene, Catal. Today 40 (1998) 353–365.
[56] S.A. Larson, J.L. Falconer, Initial reaction steps in photocatalytic oxidation of aromatics, Catal. Lett. 44 (1997) 57–65.